Supporting Information

Fluidic Lignin with Ultra-Low Glass Transition Temperature (T_g < -57 °C): A Verstile Polyelectrolyte Solvent Platform

Qiaoling Liu,[1] Yang Wang, [1] Hairong Wang,[1] Zhenhua Su,[2] Xiang Hao, and Feng Peng**

Characterization of LA

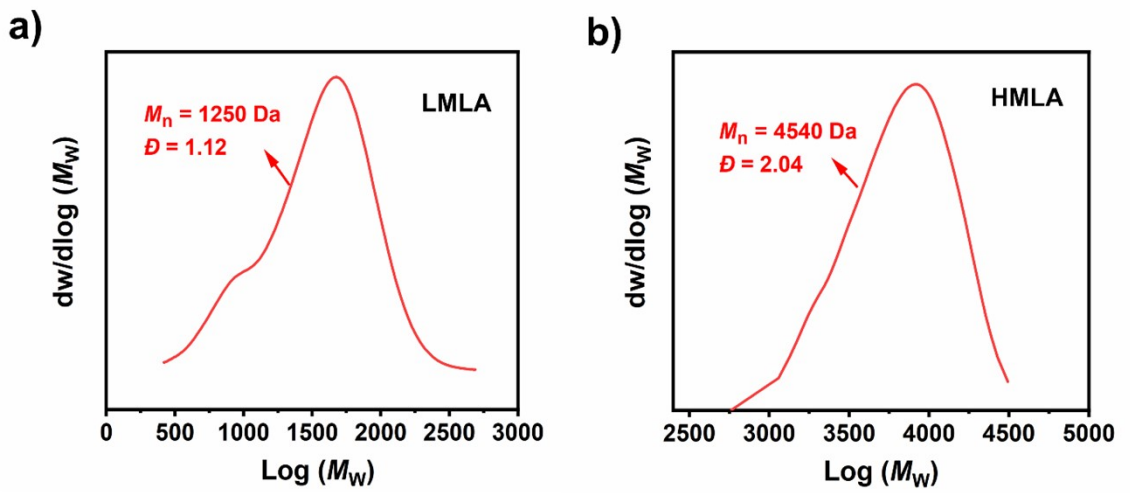

Fig. S1 GPC curves of LWLA and HWLA, respectively.

Table S1 Sulfonation degree (*DS*) of LA.

Sample	*DS* (mmol/g)	Mass fraction (%)			
		N	C	H	S
LMLA	0.15	0.00	39.73	5.78	0.49
HMLA	2.95	0.55	35.76	4.99	9.43

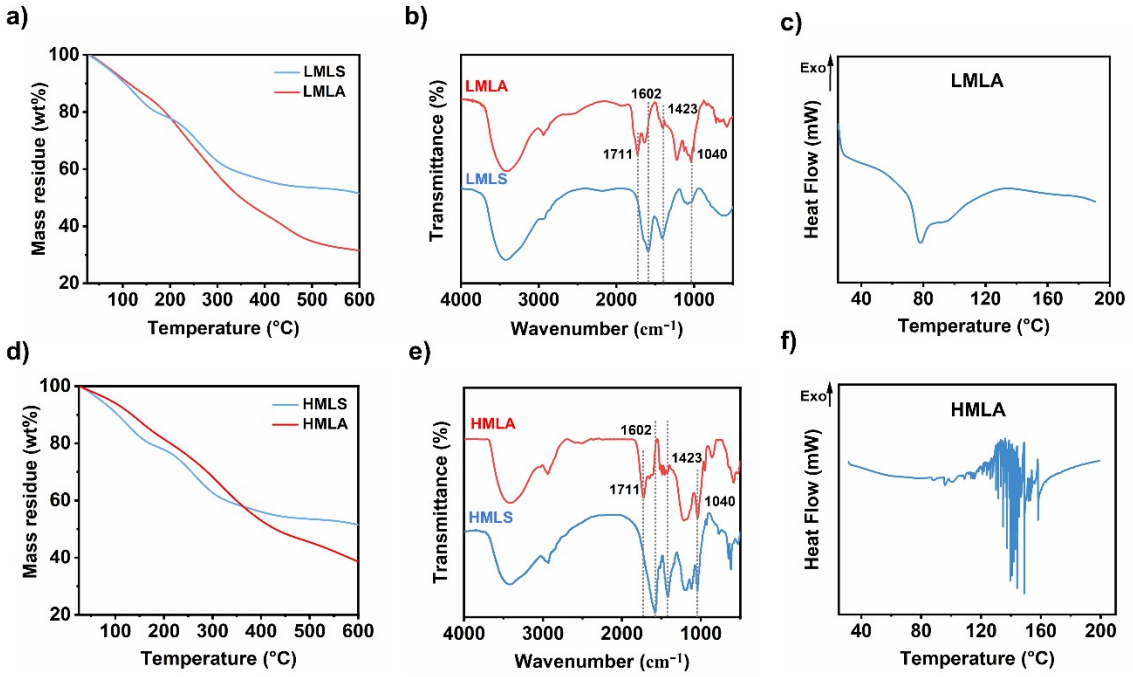

Fig. S2 Characterization properties of LA and LS. a) TGA, b) FT-IR of LMLA and LMLS. c) DSC of LMLA. d) TGA, e) FT-IR of HMLA and HMLS. f) DSC of HMLA.

Characterization of DESL

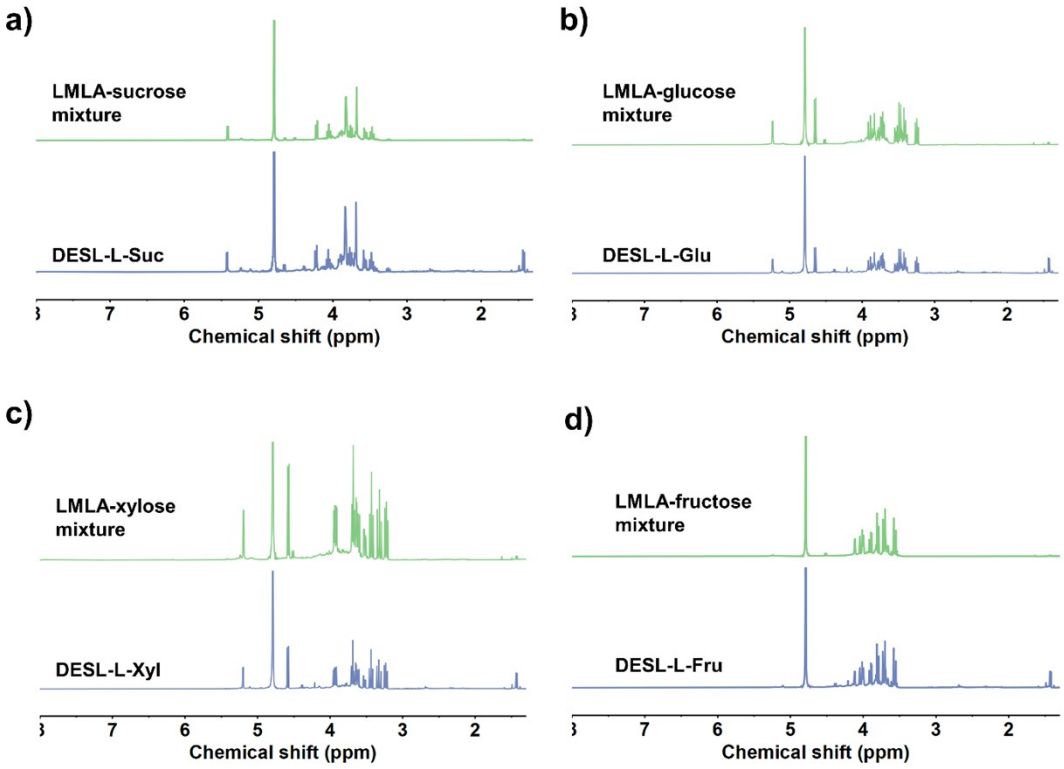

Fig. S3 ^{1}H NMR spectra of LMLA-sugars mixture and corresponding DESL.

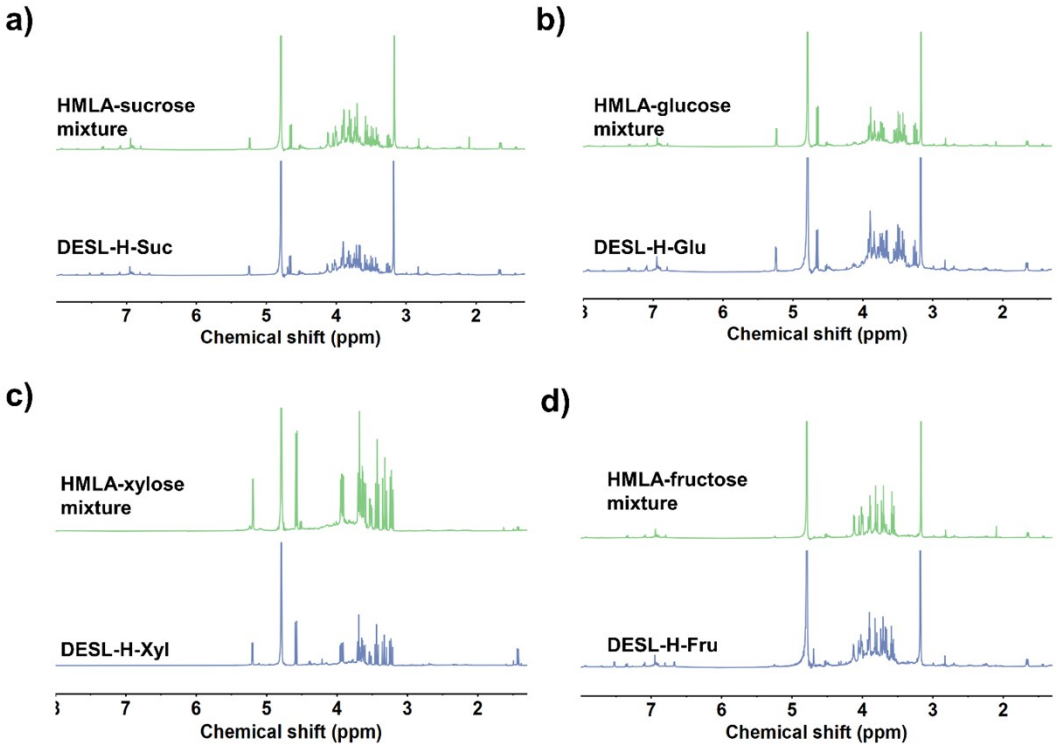

Fig. S4 ^{1}H NMR spectra of HMLA-sugars mixture and corresponding DESL.

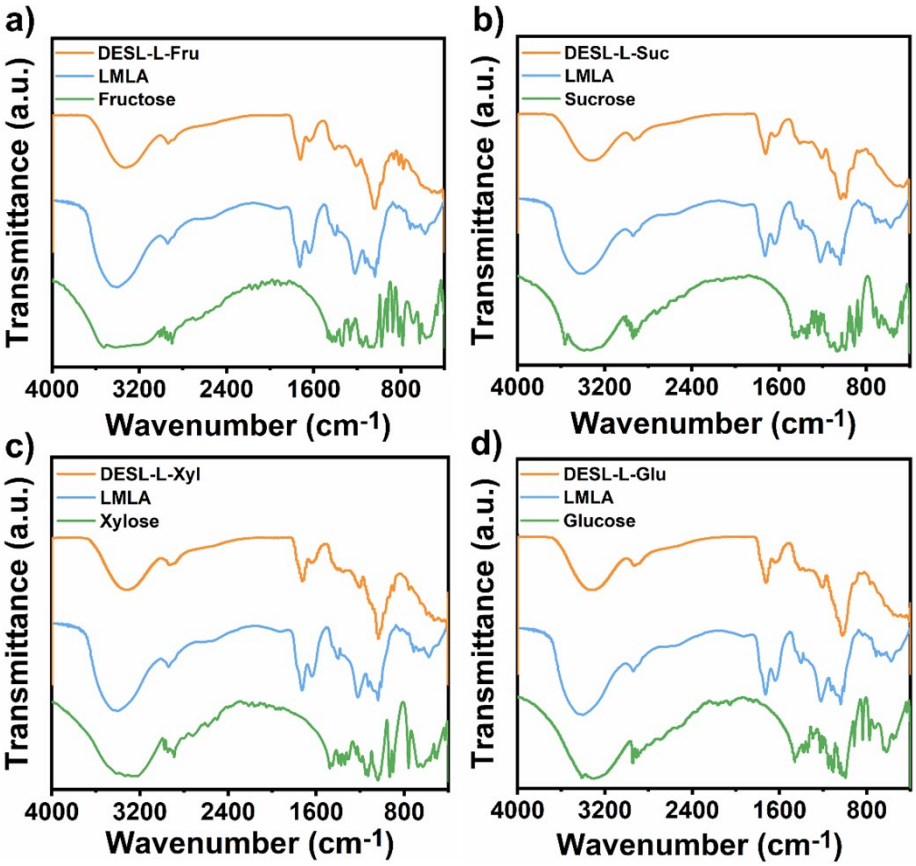

Fig. S5 FT-IR spectra of sugars, LMLA and corresponding DESL.

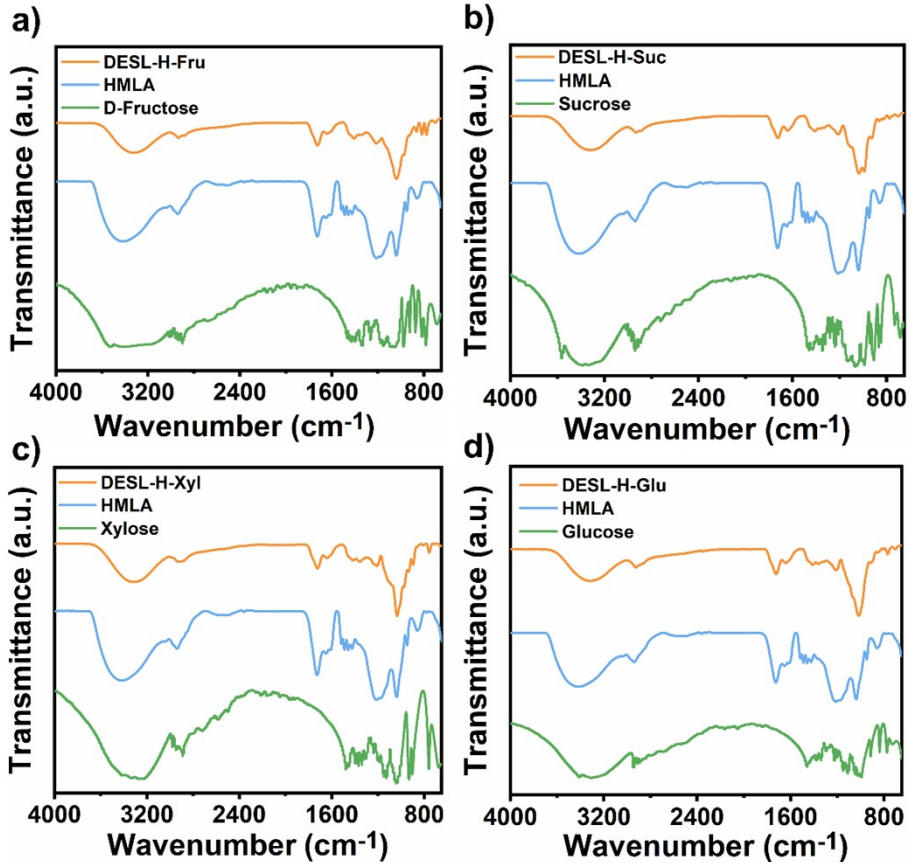

Fig. S6 FT-IR spectra of sugars, HMLA and corresponding DESL.

DFT Calculation

The best structures of the LA and D-(+)- xylose were searched using the Molclus program. The collected omplex structures were optimized using the gfn2-xtb method in the xtb software (version 6.4.1),[1,2] and the optimized structures and corresponding energy data were collected. Structures with similar energies (energy threshold = 1 kcal/mol) and similar structures (geometry threshold = 1 Angstrom) are identified as the same structure. All-electron DFT calculations have been carried out by the latest version of ORCA quantum chemistry software (version 5.0.3). The composite methods r2SCAN-3c was adopted for all geometry optimization calculations. The nature of noncovalent interaction was studied by using IGM (Independent Gradient Model) method through Multiwfn software.[3] The visualization of IGM and orbitals were rendered by VMD.[4]

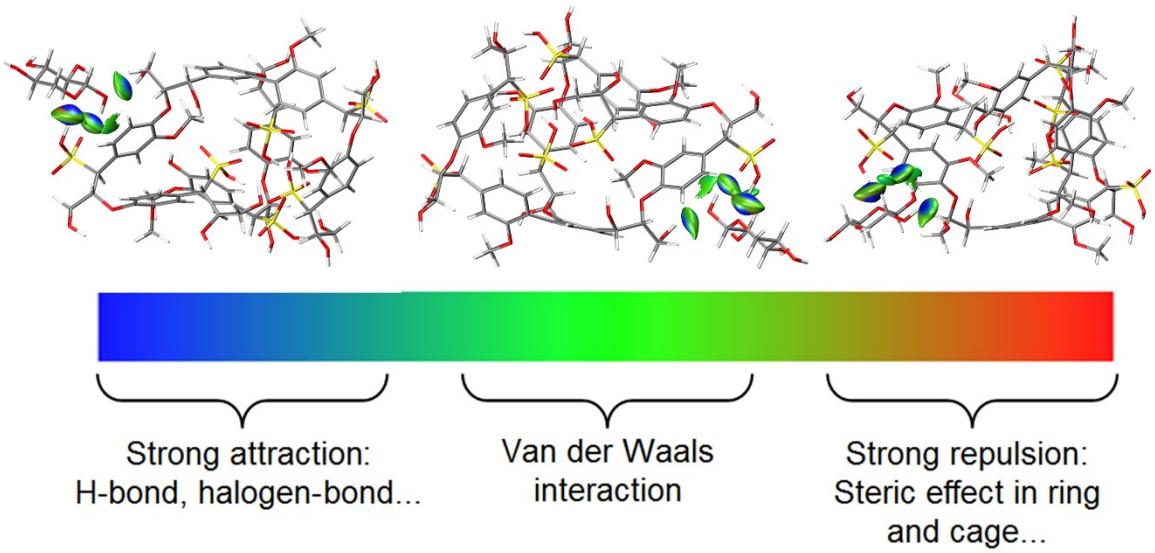

Fig. S7 The independent gradient model (IGM) isosurfaces for the interaction between LA (seven phenylpropane units) and D-(+)-xylose, and the color bar shows that blue, green, and red represent strong attraction interactions (hydrogen bonding), van der Waals interactions, and strong nonbonded overlap, respectively.

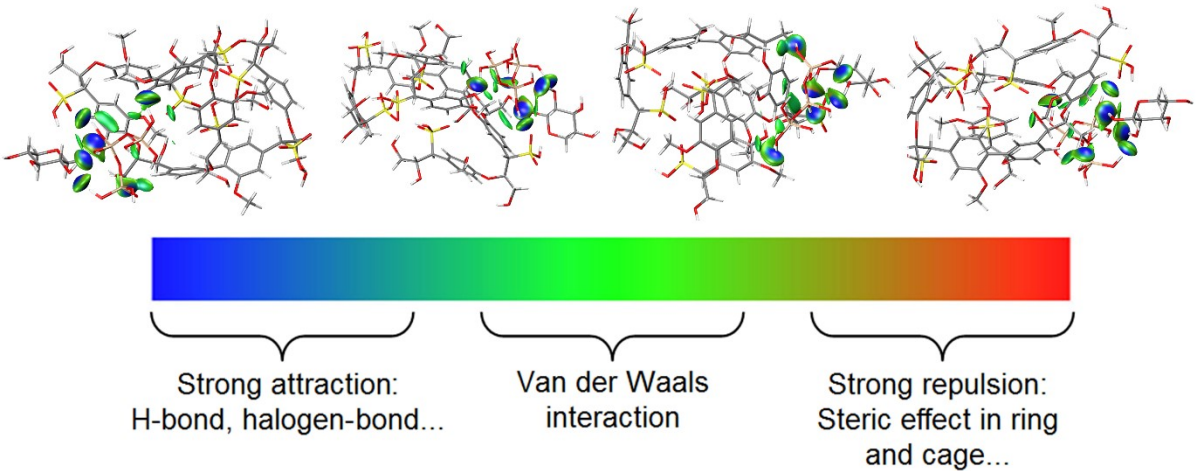

Fig. S8 The independent gradient model (IGM) isosurfaces for the interaction between LA (seven phenylpropane units) and D-(+)-xylose and glass (with $(HO)_3SiOSi(OH)_2OSi(OH)_3$ as model), and the color bar shows that blue, green, and red represent strong attraction interactions (hydrogen bonding), van der Waals interactions, and strong nonbonded overlap, respectively

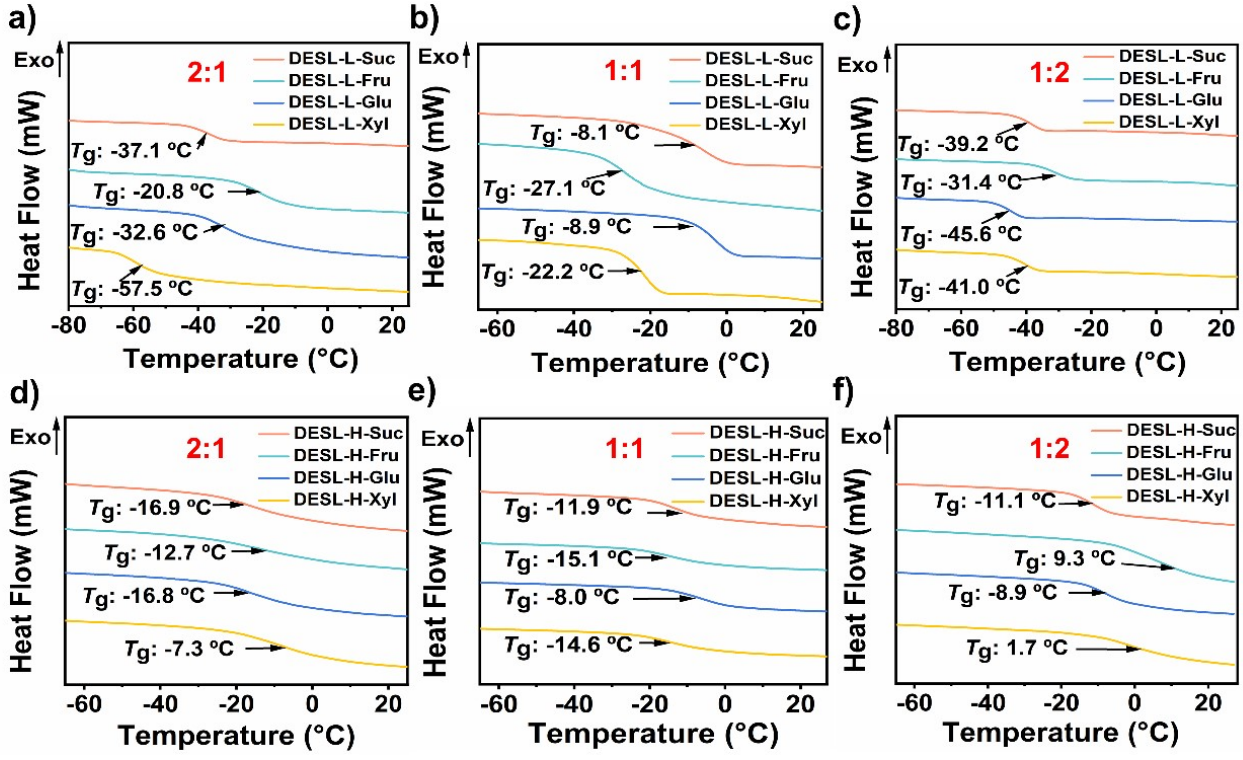

Fig. S9 Glass transition temperatures (T_g) of DESL.

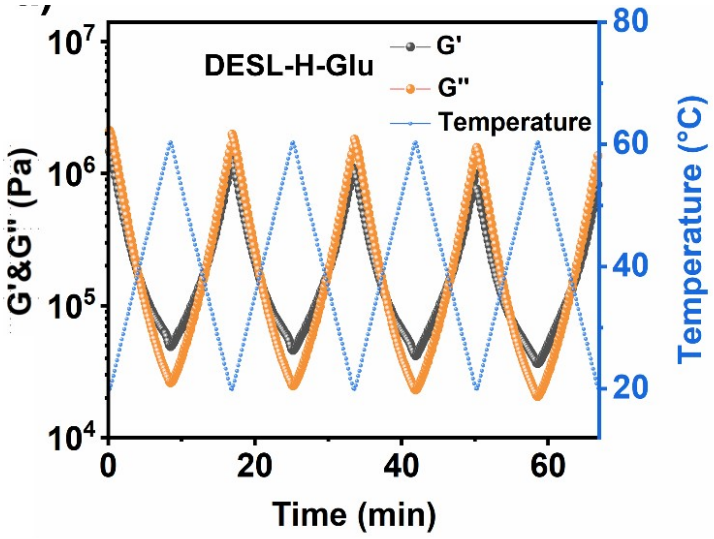

Fig. S10 Temperature-dependent moduli of DESL-H-Glu.

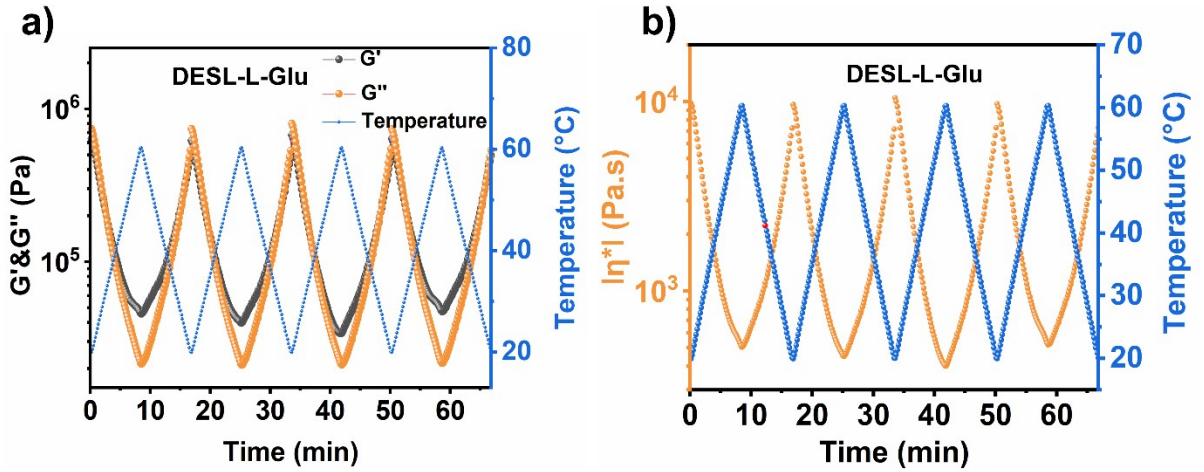

Fig. S11 Temperature-dependent moduli and composite viscosity values of DESL-L-Glu.

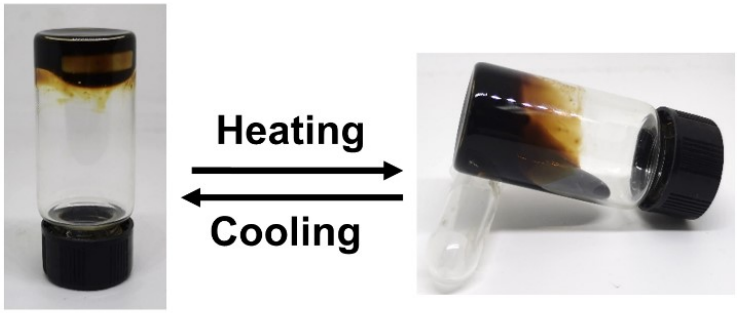

Fig. S12 Photographs of thermo-responsive behaviors of DESL.

Adhesive performance of DESL

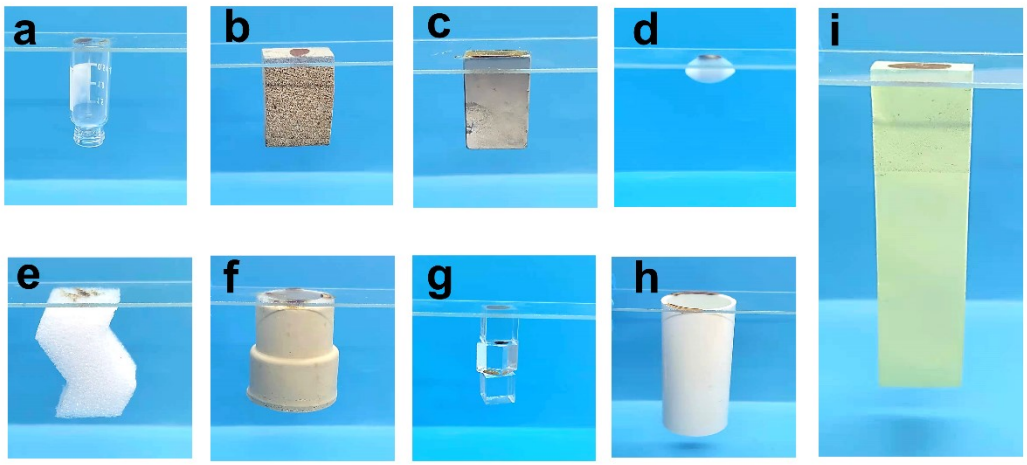

Fig. S13 Photos of DESL adhering on the surface of various substrates including a) glass, b) wood, c) steel, d) polytetraflfluoroethylene (PTFE), e) expandable polyethylene (EPE), f) rubber, g) polymeric methyl methacrylate (PMMA), h) polyvinyl chloride (PVC), and i) paper.

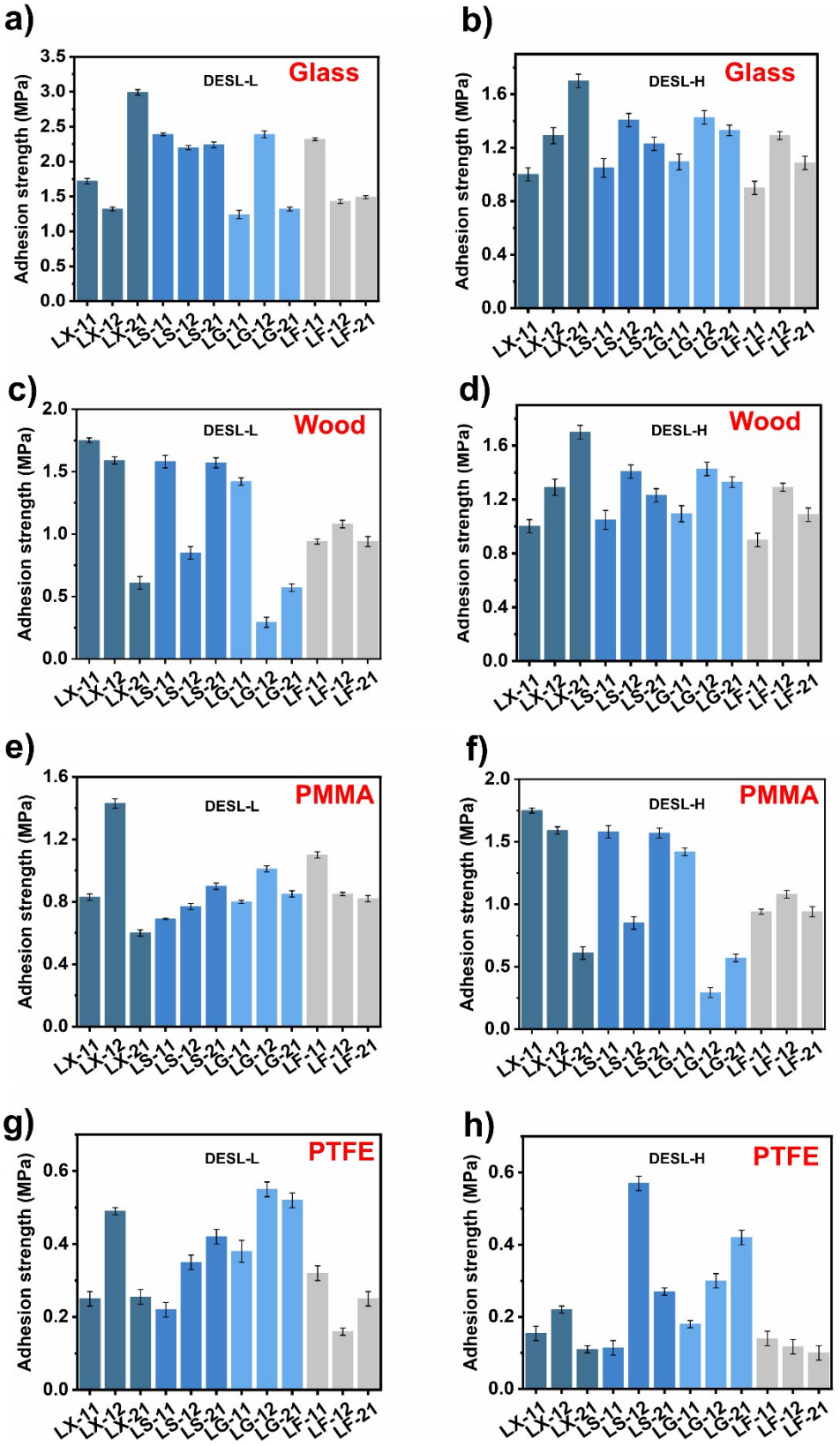

Fig. S14 Adhesion strengths of DESL on different substrate surfaces. a), c), e) and g) represented the adhesion strengths of low-molecular-weight DESL. b), d), f), and j) represented the adhesion strengths of high-molecular-weight DESL.

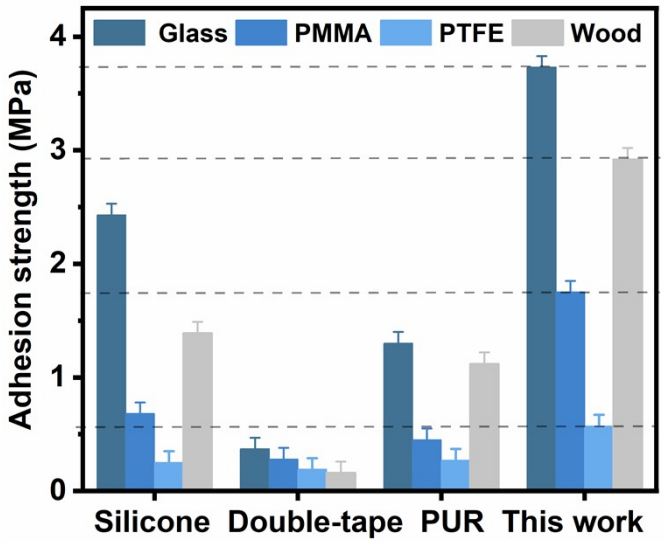

Fig. S15 Adhesion strengths of commercial adhesives and DESL on different substrate surfaces.

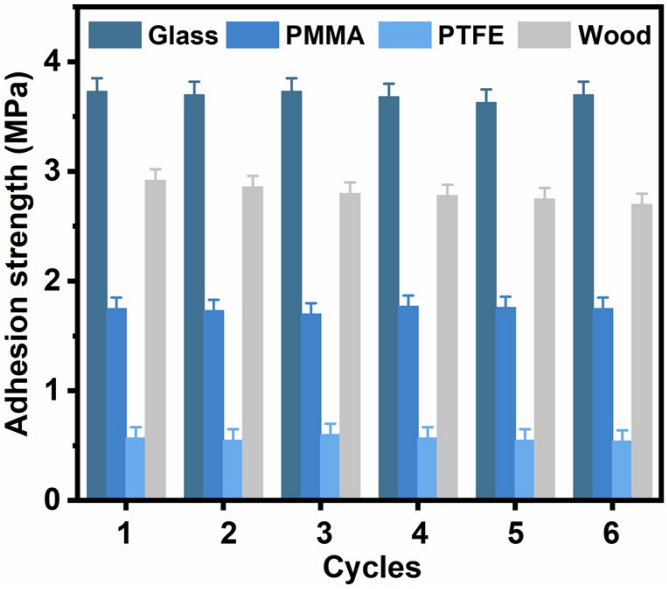

Fig. S16 Adhesion strengths of DESL-H-Glu on different substrate surfaces under multiple cycles.

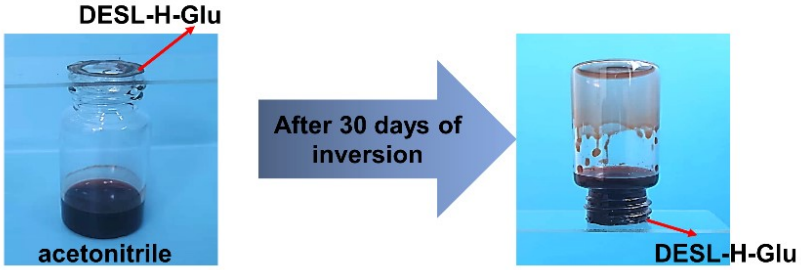

Fig. S17 Picture showing the organic solvent-resistant adhesion of DESL-H-Glu (methyl red dye was added to the acetonitrile solution to get a better view).

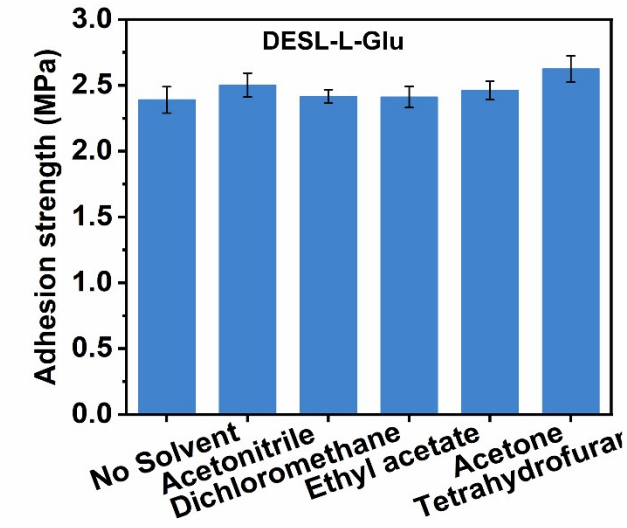

Fig. S18 Adhesion strengths of low-molecular-weight DESL-Glu on glass in different organic solvents.

Preparation and characterization of conductive adhesives

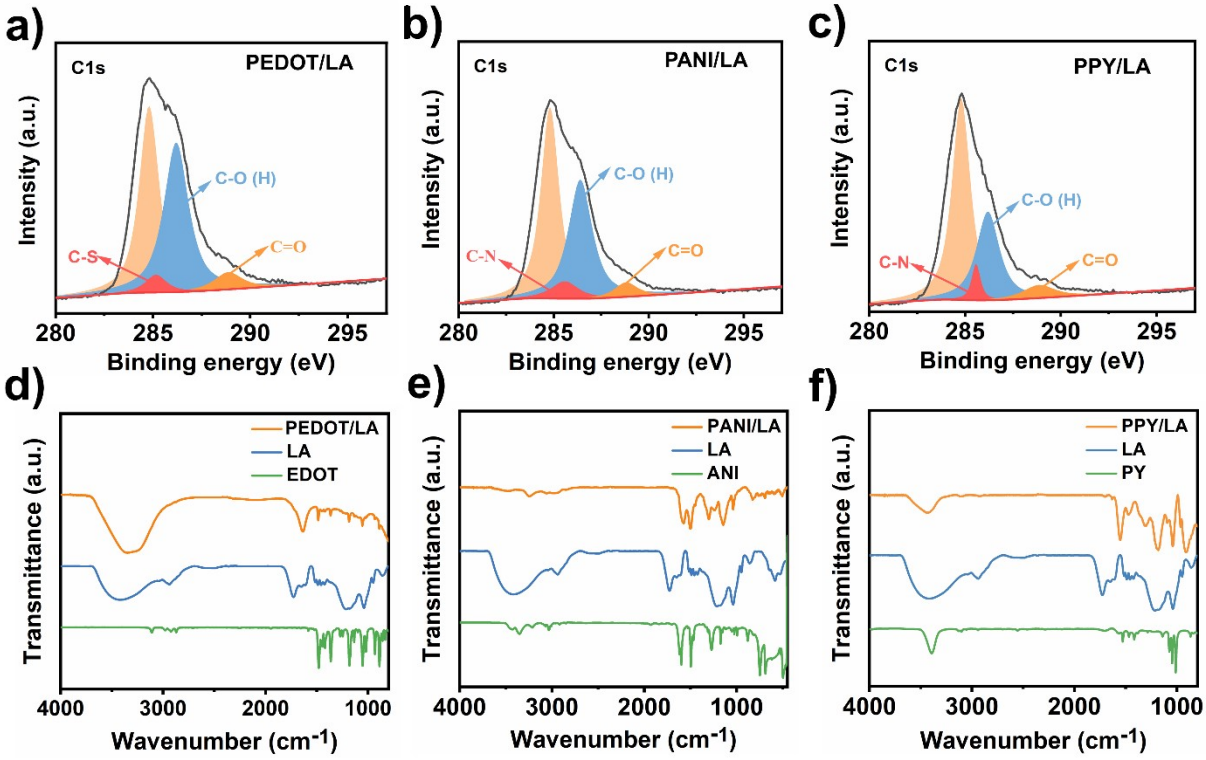

Fig. S19 XPS analysis of a) PEDOT/LA, b) PANI/LA, and c) PANI/LA nanoparticles. FT-IR spectra of d) PEDOT/LA, e) PANI/LA, and f) PANI/LA nanoparticles.

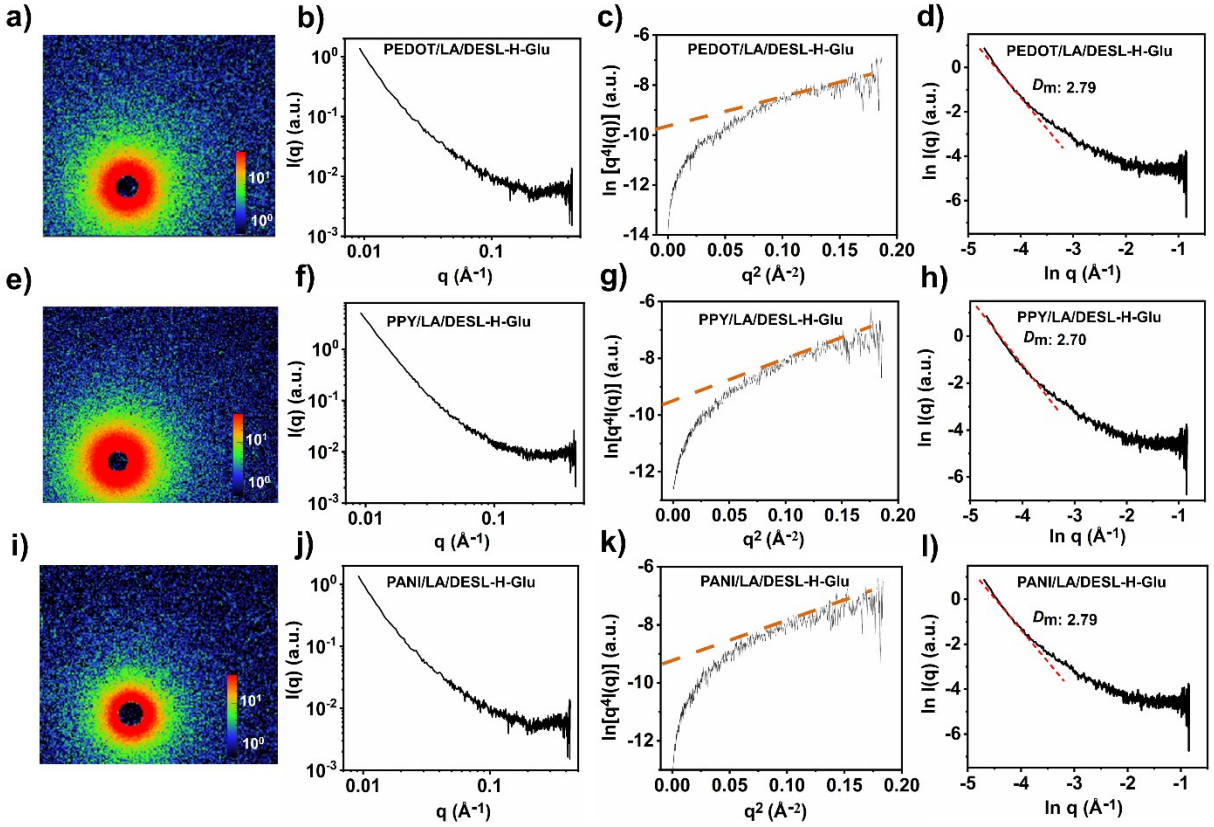

Fig. S20 a) 2D-SAXS patterns, b) SAXS pattern, c) mass fractal and d) Porod plot of PEDOT/LA/DESL-H-Glu. e) 2D-SAXS patterns, f) SAXS pattern, g) mass fractal and h) Porod plot of PPY/LA/DESL-H-Glu. i) 2D-SAXS patterns, j) SAXS pattern, k) mass fractal and l) Porod plot of PANI/LA/DESL-H-Glu.

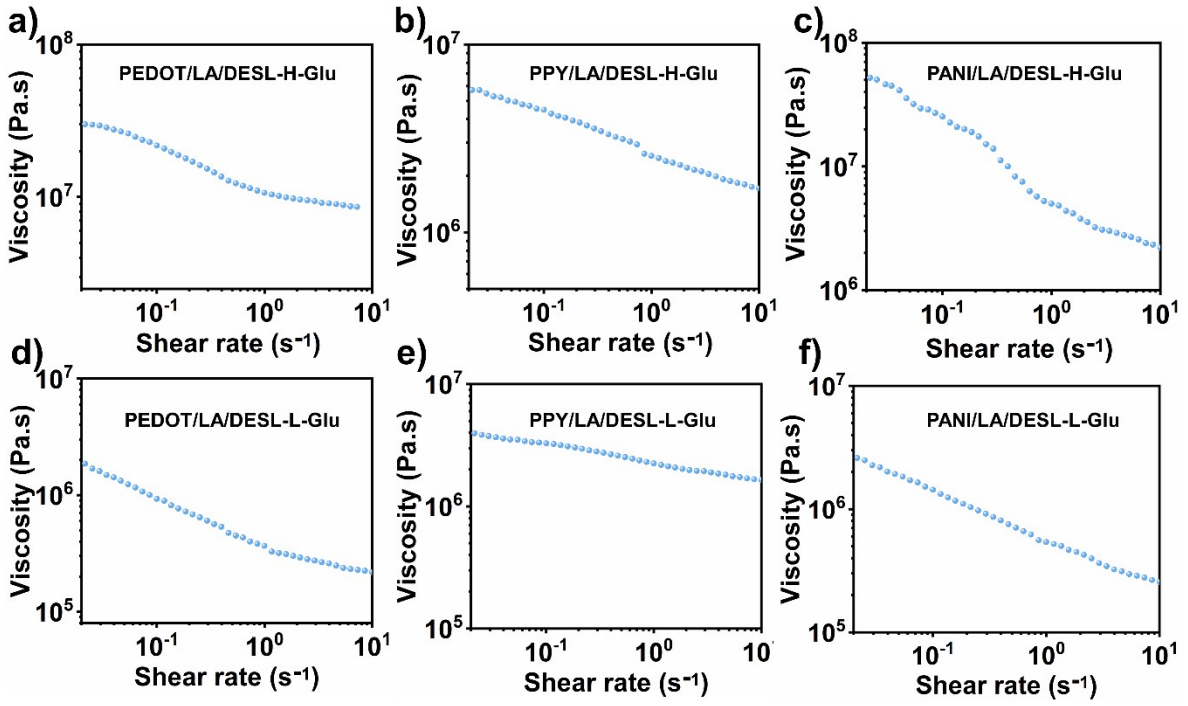

Fig. S21 Shear viscosity profile as a function of the frequency of DESL-H/L-Glu with CPs

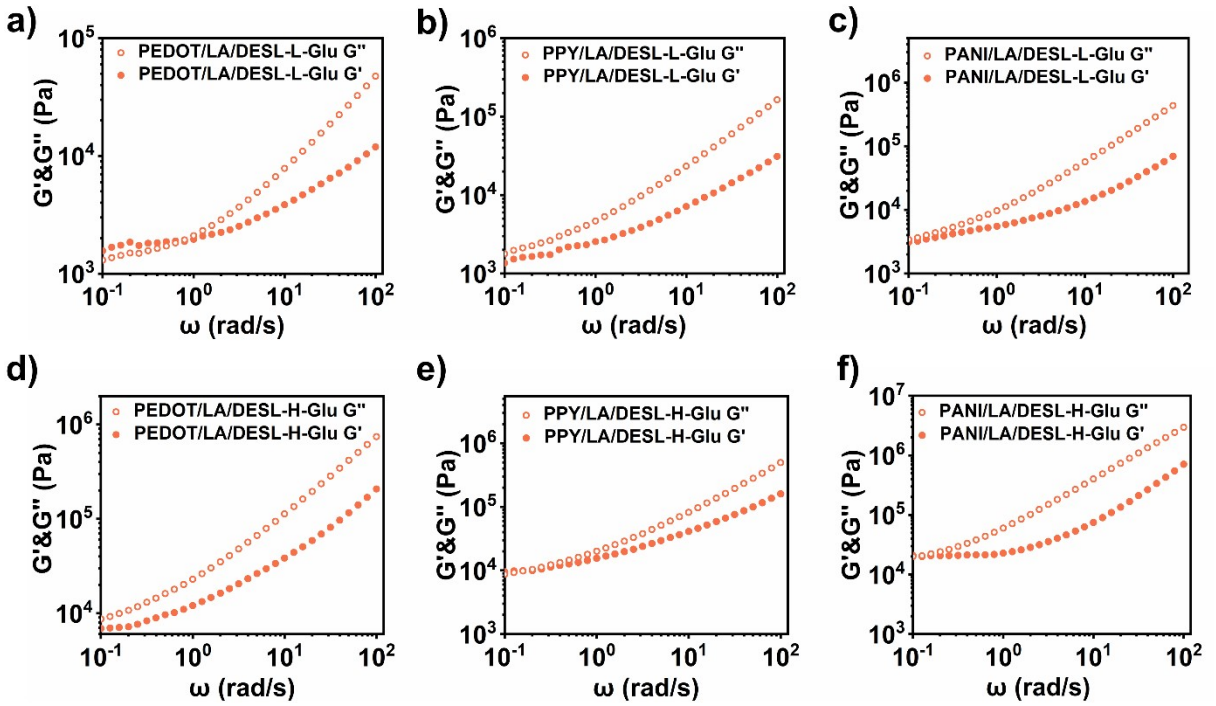

Fig. S22 Moduli variations as a function of the frequency of DESL-H/L-Glu with CPs.

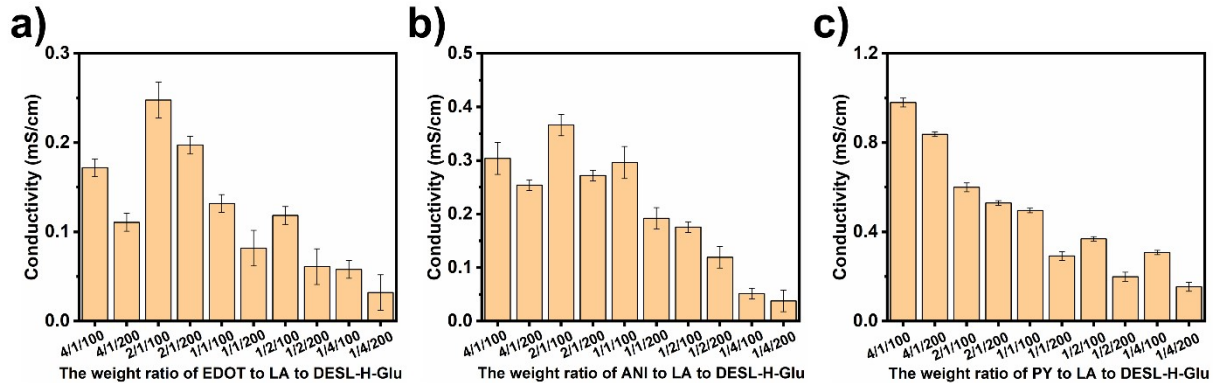

Fig. S23 The conductivity of CP/LA/DES

References

1. C. Bannwarth, S. Ehlert and S. Grimme, *J. Chem. Theory Comput*. **2019**, *15*, 1652.

2. C. Bannwarth, E. Caldeweyher, S. Ehlert, A. Hansen, P. Pracht, J. Seibert, S. Spicher, S. Grimme, *WIREs Comput. Mol. Sci.* **2020**, *11*, e01493.

3. Tian Lu, Feiwu Chen, J. *Comput. Chem*. **2012**, *33*, 580.

4. W, Humphrey, A. Dalke, K. Schulten, *J. Molec. Graphics.* **1996**, *14*, 33.